Distributed Model Predictive Control for cooperative floating object transport with multi-vessel systems

Chen, Linying; Hopman, Hans; Negenborn, Rudy R.

DOI
10.1016/j.oceaneng.2019.106515

Publication date
2019

Document Version
Accepted author manuscript

Published in
Ocean Engineering

Citation (APA)
Chen, L., Hopman, H., & Negenborn, R. R. (2019). Distributed Model Predictive Control for cooperative floating object transport with multi-vessel systems. *Ocean Engineering*, *191*, Article 106515. https://doi.org/10.1016/j.oceaneng.2019.106515

Distributed Model Predictive Control for Cooperative Floating Object Transport with Multi-Vessel Systems

Linying Chen, Hans Hopman, and Rudy. R. Negenborn

Department of Maritime and Transport Technology, Delft University of Technology, Delft, The Netherlands

Abstract

Compared to an individual Autonomous Surface Vessel (ASV), greater efficiency and operational capability can be realized by a team of cooperative ASVs for certain operations, such as search and rescue, hydrographic survey and navigation assistance. This paper focuses on cooperative floating object transport, i.e., a group of ASVs coordinate their actions to transport floating objects. We propose a multi-layer distributed control structure for the object transport system. The object transport problem is formulated as the combination of several sub-problems: trajectory tracking of the object, control allocation, and formation tracking of the ASVs. The sub-problems are integrated by a nonlinear towline model that describe the transformation of forces considering the mass and elasticity of the towline. A controller based on Model Predictive Control (MPC) is designed to control the motion of each ASV. A negotiation framework based on the Alternating Direction of Multipliers Method (ADMM) is then proposed to achieve consensus among the ASVs. Numerical simulations of utilizing the proposed cooperative system to move a large vessel sailing inbound the Port of Rotterdam are carried out to show the effectiveness of our method. Besides transporting barges and off-shore platforms, the proposed cooperative object transport system could also be a solution to coordinate non-autonomous vessels and ASVs in future autonomous ports where both human-operated and autonomous vessels exist.

Keywords: Cooperative Multi-Vessel Systems, Cooperative Floating Object Transport, Distributed Model Predictive Control, Formation control, ASV

1. Introduction

The Autonomous Surface Vessel (ASV) is an innovation to improve the safety and efficiency of waterborne transport and has become a hot topic in recent years [1, 2]. Seeing the advantages of multi-agent systems, especially efficiency gains and fault tolerance, cooperative control of multiple ASVs has gained increasing attention [3, 4, 5, 6]. Compared to an individual ASV, greater efficiency and operational capability can be realized by groups of ASVs operating in a coordinated fashion. Potential applications of Cooperative Multi-Vessel Systems (CMVSs) include transportation in urban areas, large object transport (navigation assistance), surveillance, search and rescue, etc. This paper focuses on cooperative floating object transport, i.e., a group of ASVs coordinate their actions to transport floating objects.

Cooperative object transport in Multi-Robot Systems has been studied for decades. Many coordination strategies have been proposed. A comprehensive summary of recent advancements in Multi-Robot Systems for cooperative object transport is provided in [7]. Compared with land-based robots, ASVs have different dynamics and control constraints. When controlling the motion of land-based robots, sideway speed and Coriolis force are not considered [8], while those are important factors that need to be taken into account when control vessels [9]. Therefore, adjustments are needed when applying the methods for land-based robots to control multiple ASVs.

The number of research on cooperative object transport in the field of waterborne transport is relatively small. A related topic is the manipulation of large vessels with multiple tugboats. In [10, 11, 12], control strategies that enable a barge to track a reference trajectory or orientation using a swarm of autonomous tugboats are discussed. In those papers, the tugboats are attached to the barge and apply forces at some fixed incident angles. The tugboats appear in essence as independent azimuth thrusters. In [13], the initial positions of the tugboats are arbitrary. Nonetheless, once contact is established, the location of the tugboats are time invariant. Moreover, only rotational motion is considered.

The tugs are normal to the surface of the vessel to provide torque to rotate the vessel from current orientation to the desired orientation. In those papers, the attitude of the tugboats is not considered. The heading of tugboats usually differs sharply from the path direction, which is inefficient while moving the object along the path. Besides, collision avoidance is not considered in those papers.

If physical connections between the object and ASVs and the attitude of the ASVs are considered, such as connecting the object and the ASVs using ropes, the maintaining of the geometric configuration during movement is required, i.e., formation tracking. Formation tracking aims at controlling the vessels to maintain a prescribed configuration and to follow predefined trajectories. In [14] and [15], detailed surveys on formation control of multi-agent systems are presented. In the field of maritime transport, formation tracking has attracted increasing interests, such as [16, 17, 18]. However, collision avoidance is usually not taken into account, or only considered the conflicts among the formation mates. Moreover, conventional methods, such as leader-follower and virtual structure, usually either consider obstacles before the formation is formed or use shape variation and regeneration for collision avoidance during trajectory tracking. However, when the ASVs are connected to the object, changing the formation shapes to avoid obstacles is impossible.

This paper focuses on the control problem of cooperative floating object transport, i.e., utilizing a team of ASVs to transport a larger floating object, such as a large vessel, barge, or offshore platform. The object and the ASVs are connected with towlines, and the ASVs maintain the formation when moving the object. We propose a multi-layer distributed control structure for the object transport system. With the designed scheme, the original cooperative transport problem is considered as the combination of several sub-problems: trajectory tracking of the object, control allocation and formation tracking of the ASVs. Controllers are designed using Model Predictive Control (MPC) to control the motion of the ASVs and the object. Then, an optimization-based allocation method is designed to ensure the forces that are needed to move the object are produced jointly by the ASVs. A nonlinear towline model is employed for the transformation of forces between the ASVs and the object considering the mass and the elasticity of the towline. A negotiation framework based on the Alternating Direction of Multipliers Method (ADMM) is employed to achieve consensus among the ASVs.

The contribution of this study is listed as follows: Firstly, from the perspective of concept, this paper proposes a formation-based method for transporting floating objects. The ASVs do not need frequent large attitude changes, which benefits smoother and faster object transport. Secondly, from the perspective of control algorithm design, the object transport problem is solved in a distributed fashion. The supervisory coordinator takes the feedback of the ASV controllers into account. Agreements are achieved through negotiations. Thirdly, from the perspective of communication requirements, the information that the controllers exchange consist of their predicted states. Thus, the proposed framework is suitable for negotiation among heterogeneous vessels. Moreover, in the proposed method, ASVs are connected to the object with towlines. The dynamics of the object and the towlines are taken into consideration, as well.

The remainder of this paper is organized as follows. In Section 2, we describe the cooperative object transport system being studied. The dynamic model of an ASV and a model of towline are introduced. Subsequently, the control strategy for object transport is proposed in Section 3. We design a multi-layer cooperative control scheme, and an ADMM-based DMPC framework is proposed to reach consensus on the following actions to be taken among the controllers. In Section 4, the scenarios in which the proposed cooperative system move a large vessel sailing inbound the Port of Rotterdam are simulated to show the effectiveness of the proposed method. Main findings and future research directions are provided in Section 5.

2. System Model

In this section, the model of a formation-based cooperative object transport system is constructed. The dynamic model of an ASV and a model of towline are introduced.

2.1. Dynamic model of an ASV

Cooperative object transport requires the coordination and synchronization of pushing/pulling forces by a group of ASVs in order to transport objects. In this paper, we use a triangular configuration as an example to illustrate the proposed framework. The method can also be used for other configurations.

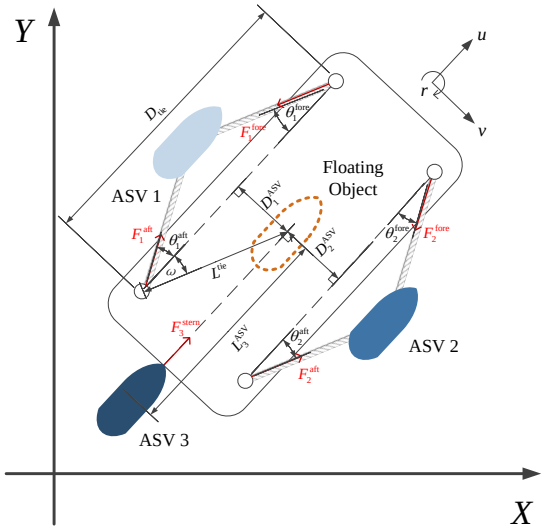

Figure 1: Configuration of the ASVs for cooperative object transport.

The geometric configuration of the ASVs is shown in Figure 1: ASV 1 and 2 are located symmetrically on the starboard side and the portside of the object; the line between the object and ASV 3 is perpendicular to the line between ASV 1 and 2. With this configuration, the surge and sway forces to move the object are provided by the three ASVs, while the moment to change the heading of the object is provided by ASV 1 and 2. Thus, the problem of object transport becomes the problem of coordinating the three ASVs to provide forces for moving the object following a reference path while keeping formation.

To calculate the forces and moment that are needed to move the object, the object is treated as a virtual vessel. The dynamics of the ASVs and the virtual vessel are described with the 3 DOF model proposed in [9]:

$$\dot{\eta}_i(t) = R\left(\psi_i(t)\right)\nu_i(t) \tag{1}$$

$$M_i\dot{\nu}_i(t) = -C_i(\nu_i(t))\nu_i(t) - D_i\nu_i(t) + \tau_i(t), \tag{2}$$

where $R(\psi_i)$ is a rotation matrix,

$$R(\psi_i(t)) = \begin{bmatrix} \cos(\psi_i(t)) & -\sin(\psi_i(t)) & 0 \\ \sin(\psi_i(t)) & \cos(\psi_i(t)) & 0 \\ 0 & 0 & 1 \end{bmatrix},$$

$\eta_i(t) = [p_i(t), q_i(t), \psi_i(t)]^{\mathrm{T}}$ are coordinates $p_i(t)$, $q_i(t)$, and heading angle $\psi_i(t)$ in the North-East-Down coordinate system; $\nu_i(t) = [u_i(t), v_i(t), r_i(t)]^{\mathrm{T}}$ are surge and sway velocities $u_i(t)$, $v_i(t)$, and yaw rate $r_i(t)$ in Body-fixed reference frame; $\tau_i(t) = [\tau_{u_i}(t), \tau_{v_i}(t), \tau_{r_i}(t)]^{\mathrm{T}}$ are forces $\tau_{u_i}(t)$, $\tau_{v_i}(t)$, and moment $\tau_{r_i}(t)$ in the Body-fixed reference frame. M_i is the system inertia matrix, including rigid-body and added mass matrices; C_i is the Coriolis-centripetal matrix, including rigid-body and added mass Coriolis-centripetal matrices; D_i is the damping force. In this paper, we consider a linear damping force.

With $x_i(t) = \left[\eta_i{}^{\mathrm{T}}(t), \nu_i{}^{\mathrm{T}}(t)\right]^{\mathrm{T}}$ and $\tau_i(t)$ the system state and input, respectively, the dynamic model (1)-(2) can be expressed as

$$\begin{aligned} \dot{x}_i(t) &= f_i\left(x_i(t), \tau_i(t)\right) \\ &= \begin{bmatrix} \mathbf{0}^{3\times3} & R_i\left(\psi_i(t)\right) \\ \mathbf{0}^{3\times3} & M_i{}^{-1}\left(-C_i(\nu_i(t)) - D_i\right) \end{bmatrix} x_i + \begin{bmatrix} \mathbf{0}^{3\times3} \\ M_i{}^{-1} \end{bmatrix} \tau_i. \end{aligned} \tag{3}$$

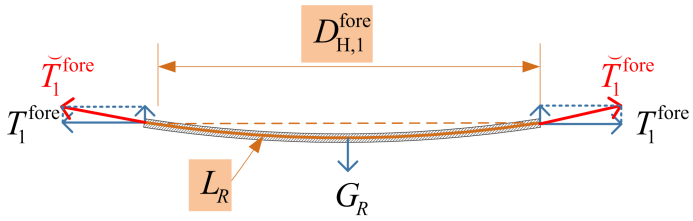

Figure 2: Tension on a towline.

In this paper, we consider a discrete dynamic model with a sample time T_s:

$$x_i(k+1) = x_i(k) + \int_{kT_s}^{(k+1)T_s} f_i\left(x_i(k), \tau_i(k)\right)dt. \tag{4}$$

2.2. Towline model

At each time step, the object, towlines and ASVs are in mechanical equilibrium. The forces provided by each ASV are applied to the towlines and the forces are transferred along the towlines to the object. In this paper, we focus on the horizontal plane. Denote the forces along the towlines on the horizontal plane as $F(k) = \left[F_1^{\text{fore}}(k), F_1^{\text{aft}}(k), F_2^{\text{fore}}(k), F_2^{\text{aft}}(k), F_3^{\text{stern}}(k)\right]^{\text{T}}$, the relation between the forces that are needed to move the object $\tau^*(k)$ and F is

$$\tau^*(k) = \Gamma(k)F(k), \tag{5}$$

where $\tau^* = [\tau_u^*, \tau_v^*, \tau_r^*]^{\text{T}}$ and $\Gamma(k)$ is the transformation matrix,

$$\Gamma(k) = \begin{bmatrix} -\cos\left(\theta_1^{\text{fore}}(k)\right) & \cos\left(\theta_1^{\text{aft}}(k)\right) & -\cos\left(\theta_2^{\text{fore}}(k)\right) & \cos\left(\theta_2^{\text{aft}}(k)\right) & 1 \\ -\sin\left(\theta_1^{\text{fore}}(k)\right) & -\sin\left(\theta_1^{\text{aft}}(k)\right) & \sin\left(\theta_2^{\text{fore}}(k)\right) & \sin\left(\theta_2^{\text{aft}}(k)\right) & 0 \\ -L^{\text{tie}}\sin\left(\theta_1^{\text{fore}}(k)+\omega\right) & L^{\text{tie}}\sin\left(\theta_1^{\text{aft}}(k)+\omega\right) & L^{\text{tie}}\sin\left(\theta_2^{\text{fore}}(k)+\omega\right) & -L^{\text{tie}}\sin\left(\theta_2^{\text{aft}}(k)+\omega\right) & 0 \end{bmatrix},$$

where $\theta_i^{\text{fore}}(k)$ and $\theta_i^{\text{aft}}(k)$ are the angles between the towlines and central line of the object, whose subscript and superscript indicate different towlines, see Figure1; ω is the angle of the segment between two ties and the center of mass of the object; L^{tie} is the distance from the center of mass of the object to the segment between the ties.

We assume that the towlines have a uniform density. Due to gravity, the towline will be shaped as a curve. In Figure 2, we use the towline that connects the fore tie at the object and ASV i as an example: T_1^{fore} is the tension in the horizontal direction; $\breve{T}_1^{\text{fore}}$ is the tension on the towline; G_R and L_R are the gravity and the length of the towline; $D_{\text{H},1}^{\text{fore}}$ is the horizontal distance between the two ends of the towline. Different models have been proposed to calculate the tension on the towline, such as in [19, 20]. In this paper, a catenary model is applied considering the mass and the elasticity of the towline [20]:

$$T_1^{\text{fore}}(k) = \left(D_{\text{H},1}^{\text{fore}}(k) - 2\frac{T_1^{\text{fore}}(k)}{\varpi}\sinh^{-1}\left(\frac{\varpi L_R/2}{T_1^{\text{fore}}(k)}\right)\right)\frac{EA}{L_R}, \tag{6}$$

where ϖ is the density of the towline; E is the so-called Young's modulus of the towline. A is the cross-sectional area of the towline.

At the same time, because ASV 1 is connected to the object with two towlines, the distances between the ASV and its connected ties should also meet the Law of Cosines, i.e.,

$$\cos\theta_1^{\text{fore}}(k) = \frac{\left(D_{\text{H},1}^{\text{fore}}(k)^2 + D_{\text{tie}}^2 - D_{\text{H},2}^{\text{aft}}(k)^2\right)}{2D_{\text{H},1}^{\text{fore}}(k)D_{\text{tie}}}. \tag{7}$$

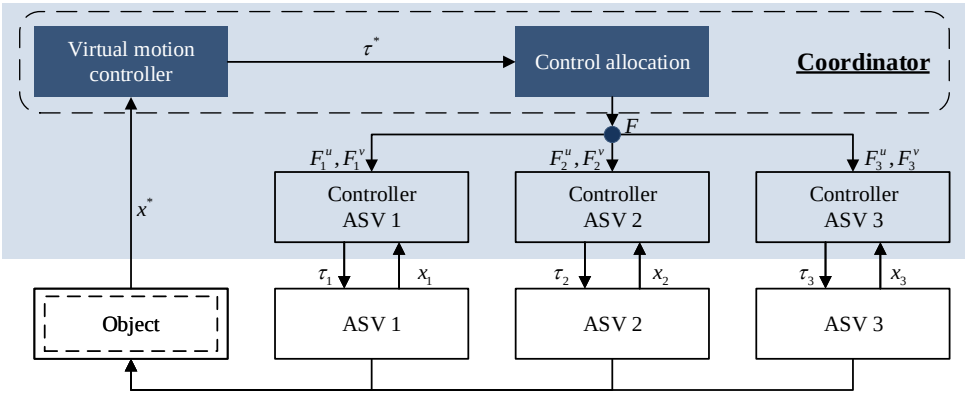

Figure 3: Multi-layer DMPC for cooperative object transport.

3. DMPC for cooperative object transport

MPC has been popular in practical applications since its early days [21]. For waterborne transport, MPC methods also have many advantages, especially when considering the predictive property of MPC methods [3]. Moreover, MPC considers the latest available measurement of the system's state and up-to-date information regarding disturbances, which provides the MPC methods the capability, to a certain extent, to be robust against disturbances. Besides, DMPC (Distributed Model Predictive Control) has many advantages for the control of large-scale networked systems [22]. Therefore, we consider DMPC as a suitable approach to carry out the task of object transport.

In this section, we propose a DMPC approach for cooperative object transport. We firstly introduce a multi-layer control structure for the object transport system. Then, we linearize the above-mentioned dynamic model to form the prediction model of the MPC controllers for the ASVs and the virtual vessel. After designing the controller for the object, an optimization-based control allocation method is presented to determine the forces that each ASV should provide. In the end, an iterative negotiation framework is provided for the cooperation of the controllers.

3.1. Control structure

Figure 3 illustrates the multi-layer structure for the control of the object transport system. A coordinator at the higher level is responsible for two tasks: one is to determine the virtual forces to control the motion of the object (τ^*); the other is to compute the forces (F_i^u and F_i^v) that ASV i should provide, which ensures that the commanded virtual control τ^* is produced jointly by the ASVs. Then, ASV controller i determines its own control τ_i according to its own state x_i while providing the rewired forces. The actions that the ASVs take decide the final state of the object, i.e., x^*. The function of the coordinator can be fulfilled either by one of the ASV controllers or an additional controller on the object or one of the ASVs or on the shore.

3.2. MPC controller design

3.2.1. Linear prediction model

The basic concept of MPC is to use a dynamic model to forecast system behavior and then optimizing the forecast to produce the best decision [23]. Therefore, at each time step, a prediction is needed. In this paper, the successively linearized model presented in [24, 25] is adopted as the prediction model for the following reasons.

- The dynamics described in (3) are highly nonlinear. In this paper, an MPC framework is used for the control of ASVs. If this nonlinear model is directly used for prediction in the MPC controller, the MPC online predictions and optimizations would be too time-consuming. In [24], a comparison on the trajectory tracking performance and computation time of ASV controller using non-linear MPC and Liner MPC shows that non-linear MPC has a much higher computational complexity, especially under larger prediction horizons than linear MPC. Moreover, In our method, agreements among the controllers are achieved through iterative negotiations. A small increase in the computation time at each iteration may make the total time too long for real-world application.

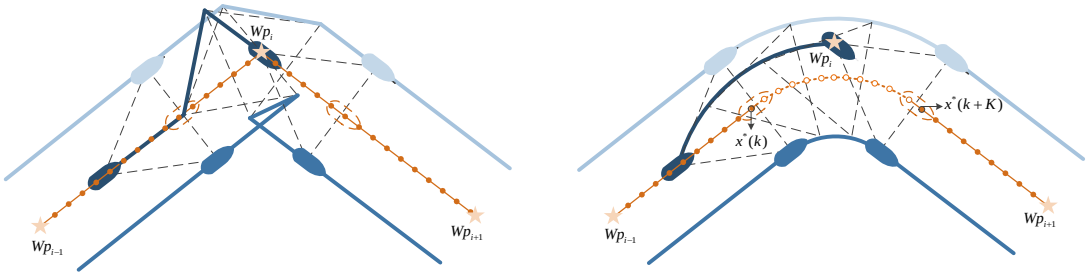

(a) Trajectory indicated by waypoints.

(b) Smooth trajectory with kinematic interpolation.

Figure 4: Reference trajectory generation.

- Different from conventional linearization method, the successively linearized method approximate the dynamics based on the seed state calculated in each time step over the prediction horizon. The actual state usually does not change much from the seed state. Therefore, it can provide a good approximation to the nonlinear dynamics of ASVs. We have carried out an analysis of the linearization errors in Appendix A, which shows that the linearized model can provide adequate accuracy for the control of ASVs.
- In this paper, we adopt a dynamic model of marine surface vehicles with three DOFs (surge, sway, and yaw) proposed in [9]. This model has been widely used for the motion control of ASVs. Various models have been proposed to describe the dynamics of vessels, such as holonomic models, kinematic models, and dynamic models [26]. However, no models can predict the dynamics of the vessels operating in real-life environments without any error, as the dynamics are influenced by many factors, such as the shape of the hull, and dimensions. Even for a vessel, its dynamics can be varying with different loads, depth of the waterways, and so on [27, 28]. The aim of this research is not to construct the most accurate dynamic model, but to develop a method that can work under the situation that the actual states of an ASV differ from the states that a mathematical model describes.
- In the proposed MPC framework, the controller calculates at each time step a sequence of control inputs for the whole prediction horizon, after which the control input for the first control sample will be implemented. Thus, at each time step, the controller will take corrective actions if the actual state differs from the predicted state.

At each time step, as a start point, the control sequence computed in last time step is shifted one sample with an additional of zeros at the end. Using this extended control sequence as seed input $\tau^e(k)$, we can obtain the seed state $x^e(k)$ with (3). By applying Taylor's theorem, we can obtain the approximation state of the ASV at $k+1$, $x_i(k+1|k)$, with following discrete linearized model:

$$x_i(k+1|k) = x_i^e(k+1|k) + A_i^{\mathrm{d}}(k|k)\Big(x_i(k|k) - x_i^e(k|k)\Big) + B_i^{\mathrm{d}}(k|k)\Big(\tau_i(k|k) - \tau_i^e(k|k)\Big), \tag{8}$$

where $A_i^d(k|k) = \left.\dfrac{\partial f_i}{\partial x_i}\right|_{\substack{x_i^e(k|k)\\ \tau_i^e(k|k)}}$, $B_i^d(k|k) = \left.\dfrac{\partial f_i}{\partial \tau_i}\right|_{\substack{x_i^e(k|k)\\ \tau_i^e(k|k)}}$ are the Jacobian matrices.

3.2.2. Reference trajectory generation

To calculate the forces and moment that are needed to make the object following a predetermined path, the object is regarded as a virtual vessel in the cooperative system, whose dynamics can be described using (3). One of the tasks of the coordinator is to control the motion of this virtual vessel to track a predetermined path.

The reference path is usually generated by discretizing segments between the waypoints with the double integrator dynamics and a constant speed $\hat{v}$, i.e., $P_i(k+1) = P_i(k) + \hat{v}$, $P_i(k)$ is the reference position at k, see the orange dots in Figure 4(a).

In the task of object transport, the ASVs keep formation while navigating. The reference state that each ASV should track includes reference trajectory and heading, i.e., $w_i(k) = [P_i(k)^{\mathrm{T}}, \psi_i(k)]^{\mathrm{T}}$. The initial reference trajectory can be calculated according to the geometric relations shown in Figure 1, and the reference heading of the ASVs is equal to the required heading of the object, denoted as

$$w_i(k) = g_i\left(w^*(k)\right). \tag{9}$$

However, if we connect the waypoints directly, there might be abrupt changes in the trajectories of the ASVs, see Figure 4(a). Thus, we smooth the connection between two segments with kinematic interpolation [29].

After discretizing the segments with the double integrator dynamics, a connection between a start state in the segment $Wp_{i-1} \rightarrow Wp_i$ and an end state in the segment $Wp_i \rightarrow Wp_{(i+1)}$ is made with a changing velocity. The acceleration during this period K is formulated as a linear function of time in order to describe object acceleration as smooth motion, i.e., $a(t) = b + mt$. The position and velocity can be expressed as

$$p(t) = p_0 + \int_0^t v(t)dt, \tag{10}$$

$$v(t) = v_0 + \int_0^t (b + mt)dt, \tag{11}$$

where $v(t)$ is the corresponding velocity.

Accordingly, given the start position and velocity $[P(k), v(k)]$ and the end position and velocity $[P(k+K), v(k+K)]$, we can obtain a smooth connection between two segments without any abrupt changes in speed or direction, see Figure 4(b).

The smoothed reference trajectory between origin and destination is represented by a sequence of positions. The trajectory of each ASV can be calculated by (9), accordingly. At each time step, each ASV controller and coordinator finds the reference position which is closest to its current position and use the subsequent positions over the predictive horizon as the reference trajectory.

3.2.3. Control Problem

The virtual control effort that is required to control the object to track the reference trajectory are determined by solving the primal optimization problem:

$$\begin{aligned}
\text{minimize} \quad & J^*\left(\tau^*(k)\right) = \sum_{l=1}^{H_p} \Big(\alpha^* \|\eta^*(k+l\,|k) - w^*(k+l)\|_2^2 \\
& \qquad\qquad + \gamma^* \|\tau^*(k+l-1\,|k)\|_2^2\Big) && (12)\\
\text{subject to} \quad & \forall i \in \mathcal{V}, \forall l \in H_{\mathrm{p}}: \\
& x^*(k\,|k) = x^*(k), && (13)\\
& v^*_{\min} \leqslant v^*(k+l\,|k) \leqslant v^*_{\max}, && (14)\\
& \tau^*_{\min} \leqslant \tau^*(k+l\,|k) \leqslant \tau^*_{\max}, && (15)\\
& d_{*i|*}(k+l\,|k) \geqslant d_{*i,\mathrm{safe}}, && (16)\\
& P^*(k+l\,|k) \in \Xi, && (17)\\
& \text{dynamics described by (8) over the predictive horizon,} && (18)
\end{aligned}$$

where α and γ are the weights; H_{p} is the prediction horizon; l is the lth time step in the prediction horizon; $\eta^*(k+l\,|k)$ is the prediction made at time step k about the position and heading of the object at time step $k+l$; $w^*(k+l)$ is the reference at time step $k+l$, including trajectory and heading; $d_{*i|*}(k+l\,|k)$ is the distance between ASV i and the object with the information sent by ASV i, $d_{*i|*}(k+l\,|k) = \left\|P^*(k+l\,|k) - P_{i|*}(k+l\,|k)\right\|_\infty$; $P^*(k+l\,|k)$ is the prediction made at time step k about the position of the object at time step $k+l$, and $P_{i|*}$ is the position of the ASV i that the object received; $d_{*i,\mathrm{safe}}$ is the safety distance of the object; Ξ is a set of position in navigable waters, i.e., spaces

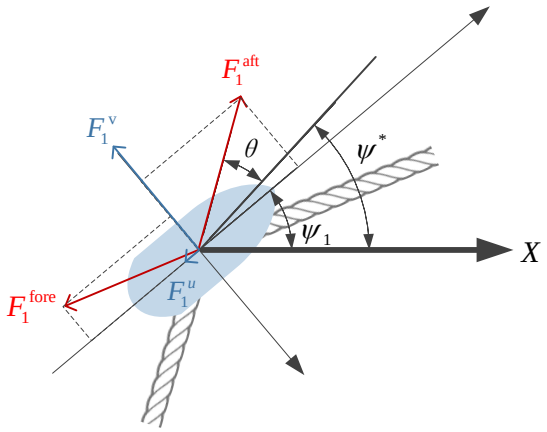

Figure 5: Force diagram of ASV 1.

which are collision-free considering static obstacles; $\tau^*(k)$ indicates control input over the prediction horizon, i.e., $\tau^*(k) = [\tau^*(k\,|k)^{\mathrm{T}}, \tau^*(k+1\,|k)^{\mathrm{T}}, \cdots, \tau^*(k+H_{\mathrm{p}}-1\,|k)^{\mathrm{T}}]^{\mathrm{T}}$.

This problem (12)-(17)can be transferred into a mixed integer linear programming problem when the collision avoidance constraint (16) is rewritten with binary variables. Details can be found in [3].

3.3. Control allocation

The virtual control effort that needed to move the object, $\tau^*(k)$, is provided by the 3 ASVs through the towlines. There is actuator redundancy when considering the whole system, i.e., the cooperative object transport system is an over-actuated system. Here, we use an optimization-based allocation method to compute a control input that ensures that the commanded virtual control $\tau^*(k)$ is produced jointly by the ASVs.

We formulate the control allocation objective function as minimize the forces along the towlines, considering the total forces that the ASVs can provide, while producing required forces. Thus, solving the control allocation problem involves solving following nonlinear optimization problem:

$$\text{minimize} \quad \sum_{l=1}^{H_p} \left\| F(k+l\,|k) - \hat{F} \right\|_2^2 \tag{19}$$

$$\text{subject to} \quad \forall i \in \mathcal{V}, \forall l \in H_{\mathrm{p}}:$$

$$\tau^*(k+l\,|k) = \Gamma(k+l\,|k) F(k+l\,|k), \tag{20}$$

$$0 \leqslant F(k+l\,|k) \leqslant F_{\max}, \tag{21}$$

$$\theta_{\min} \leqslant \theta_i^{\text{fore/aft}}(k+l\,|k) \leqslant \theta_{\max}; \tag{22}$$

$$D_{\mathrm{H,min}} \leqslant D_{H,i}^{\text{fore/aft}}(k+l\,|k) \leqslant D_{\mathrm{H,max}}; \tag{23}$$

$$\text{Towline model described by (6) and (7),} \tag{24}$$

where, $F(k+l\,|k)$ is the prediction made at k about the forces transferred by the towlines at time step $k+l$; $\hat{F}$ is the forces that transferred by the towlines when $\tau^* = 0$ while the ASVs are keeping a preferred configuration. Γ is the transformation matrix between τ^* and F; $F_{\max}$ is the maximum forces on the towline.

Subsequently, the forces each ASV should provide can be decomposed into two components in surge and sway directions (F_i^u, F_i^v) in its own body-fixed frame. Figure 5 illustrate the decomposition using ASV 1 as an example,

i.e.,

$$\begin{bmatrix} F_i^u(k) \\ F_i^v(k) \end{bmatrix} = \mathrm{T}_i(\psi_i(k), \psi^*(k)) \begin{bmatrix} F_i^{\mathrm{fore}}(k) \\ F_i^{\mathrm{aft}}(k) \end{bmatrix},$$

where $\mathrm{T}_i(\psi_i(k), \psi^*(k))$ is the transformation matrix,

$$\mathrm{T}_i(\psi_i(k), \psi^*(k)) = \begin{bmatrix} -\cos\left(\theta_i^{\mathrm{fore}}(k) + \Delta\psi_i(k)\right) & \cos\left(\theta_i^{\mathrm{aft}}(k) - \Delta\psi_i(k)\right) \\ -\sin\left(\theta_i^{\mathrm{fore}}(k) + \Delta\psi_i(k)\right) & -\sin\left(\theta_i^{\mathrm{aft}}(k) - \Delta\psi_i(k)\right) \end{bmatrix}, \tag{25}$$

where $\Delta\psi(k) = \psi_i(k) - \psi^*(k)$. For smoother and more efficient object transport, the reference heading of the ASVs and the objects are set as the desired heading of the object, i.e., the path direction. Therefore, the differences between the heading of the object and the ASVs are small, i.e., $\Delta\psi_i(k) \approx 0,\ \forall k$, and small-angle approximation can be used to simplify (25).

For each ASV, it should not only follow its own reference trajectory to keep the required related distance with the object, but also provide required forces to move the object. Accordingly, the control problem that the ASV controller i needs to solve is

$$\begin{aligned}
\text{minimize} \quad & J_i\left(\tau_i(k)\right) = \sum_{l=1}^{H_\mathrm{p}} \Big(\alpha \|\eta_i(k+l\,|k) - w_i(k+l)\|_2^2 \\
& \qquad + \gamma \|\tau_i(k+l-1\,|k)\|_2^2\Big) && (26) \\
\text{subject to} \quad & \forall i, j \in \mathcal{V},\ i \neq j, \forall l \in H_\mathrm{p}: \\
& \nu_{i,\min} \leqslant \nu_i(k+l\,|k) \leqslant \nu_{i,\max}, && (27) \\
& \tau_i(k+l\,|k) + F_i^{\mathrm{tow}}(k+l\,|k) \geqslant \tau_{i,\min}, && (28) \\
& \tau_i(k+l\,|k) + F_i^{\mathrm{tow}}(k+l\,|k) \leqslant \tau_{i,\max}, && (29) \\
& R^{-1}\left(\psi^*(k+l\,|k)\right)\eta_i(k+l\,|k) \geqslant P_i^* - \varepsilon^{\mathrm{con}}, && (30) \\
& R^{-1}\left(\psi^*(k+l\,|k)\right)\eta_i(k+l\,|k) \leqslant P_i^* + \varepsilon^{\mathrm{con}}, && (31) \\
& d_{ij|i}\left(k+l\,|k\right) \leqslant d_{\mathrm{ij,safe}}, && (32) \\
& P_i(k+l\,|k) \in \Xi, && (33) \\
& \text{dynamics described by (8) over the predictive horizon,}
\end{aligned}$$

where $F_i^{\mathrm{tow}}(k+l\,|k)$ indicates the prediction at k about the forces made that the ASV i provide at $k+l$, $F_i^{\mathrm{tow}}(k) = \left[F_i^u(k), F_i^v(k), 0\right]$; P_i^* is the corresponding position of ASV i in the Body-fixed reference frame of the object according to desired configuration and the towline model (6). For example, for ASV 1, after calculating $D_{\mathrm{H},1}^{\mathrm{aft}}(k)$, the distance between the tie and the center of mass of the ASV 1, according to the tension on the towline, the position of ASV 1 can be calculated as

$$P_1^*(k) = D_{\mathrm{H},1}^{\mathrm{aft}}(k) \begin{bmatrix} -\cos\left(\theta_1^{\mathrm{fore}}(k)\right) \\ \sin\left(\theta_1^{\mathrm{fore}}(k)\right) \\ 0 \end{bmatrix} + \begin{bmatrix} L_1^{\mathrm{ASV}} \\ D_{\mathrm{tie}}/2 \\ 0 \end{bmatrix}, \tag{34}$$

where D_{tie} is the length between two ties that are connected to ASV 1.

In constraints (30) and (31), we set a tolerance for formation keeping for the following reasons. Firstly, the ASVs and the object are connected with ropes. The ASVs are possible to have small fluctuations around the desired positions. Secondly, in the optimization, we use a linearized model to predict the dynamics of the ASVs and the object. The actual states inevitably differ from the predictions. The tolerance can help to avoid the situation that the optimization problem at the first iteration is infeasible at each time step. Thirdly, the tolerance relaxes the need for formation keep, which can help to avoid frequent control changes and is beneficial for fast convergence to the agreements.

3.4. Cooperative framework

3.4.1. Combined overall control problem

The ideal situation is that the ASVs follow the reference state and provide the required force that the coordinator informs them. However, the ASVs may fail to follow the reference paths when providing the required forces due to actuator saturation or other physical limitations. As we mentioned in Section 2, the positions of the ASVs determine the final position of the object. This means that when the ASVs cannot achieve the desired state, the object cannot achieve its desired state, either. Thus, the forces needed to move the object also change, and so are the forces each ASV needs to provide. Therefore, the ASV controllers and the coordinator needs to negotiate with each other to reach an agreement.

The agreements among the ASVs are achieved when the expected trajectory of the object calculated based on the ASVs and the predicted trajectory that the coordinator calculated become consensus. Therefore, the combined overall control problem for the object transport system can be formulated as

$$\begin{aligned} \text{minimize} \quad & \sum_{i=1}^{3} J_i\left(\tau_i(k)\right) + J^*\left(\tau^*(k)\right) && (35) \\ \text{subject to} \quad & \forall i \in \mathcal{V}: \\ & \eta_i(k) = h_i\left(\eta^*(k)\right), && (36) \\ & \eta^*(k) = h_i^{-1}\left(\eta_i(k)\right), && (37) \end{aligned}$$

where (36) indicates that the predicted trajectory of ASV i equals the expected trajectory calculated according to the predicted trajectory of the object and their geometric relation; and vice versa, (37) indicates the the predicted trajectory of the object equals the expected trajectory of the object calculated according to the predicted trajectory of ASV i. $h_i(\cdot)$ indicate the geometric relation between the object and the ASVs considering the desired formation and the towline model described by (6) and (7).

3.4.2. ADMM-based multi-layer negotiation framework

ADMM has been widely used for consensus problems with separable objective functions [30]. ADMM scheme takes the form of a decomposition-coordination procedure, in which the solution is found through iterations of solving some sub-problems.

The objective function in (35) can be separated into two parts related to local trajectory following of the ASVs and the shared trajectory following of the object. We introduce two interconnecting variables to link the two problems: the expected trajectory of the ASV i that calculated according to the predicted trajectory of the object, $z_i^*(k) = h_i^{-1}\left(\eta_i(k)\right)$; the expected trajectory of the object that calculated according to the predicted trajectory of ASV i, $z_i(k) = h_i\left(\eta^*(k)\right)$. The agreements among the ASVs and the coordinator are achieved in the following iterative way:

Except for Step 2, every step is carried out independently in parallel for each ASV i. The controllers use the information about the interconnecting variables from the most recent iteration.

4. Numerical Simulations

In this section, numerical simulations of the scenarios in which the proposed cooperative system move a large vessel sailing inbound the Port of Rotterdam are carried out to show the potential of the proposed approach. Both static and dynamic obstacles are considered in the simulation. We compare the results of two settings: one is constant configuration ignoring the dynamics of towlines; the other is time-varying configuration considering the nonlinear towline model.

Simulations are carried out with Matlab 2016a. The linear optimization problems of the controllers are solved by ILOG CPLEX Optimization Studio (Version 12.6.3), and the nonlinear optimization problems are solved by IPOPT [31], with the solution that is found in the former iteration as a starting point. The simulations are run on a PC with a dual-core 3.2 GHz Intel(R) Core(TM) i5-3470U CPU and 8 GB of RAM.

Algorithm 1 Multi-layer negotiation framework for CFOT

1: ASV controller i determines its own predicted trajectory by solving following problem:

$$\tau_i^s(k) := \underset{\tau_i(k)}{\arg\min}\, J_i\left(\tau_i(k)\right) + \lambda_i^{s-1}(k)'\left(\eta_i(k) - z_i^{s-1}(k)\right) + \rho_i/2 \ \left\|\eta_i(k) - z_i^{s-1}(k)\right\|_2^2,$$
$$\text{subject to (14)-(17),}$$

where ρ_i is penalty parameter and $\lambda_i(k)$ is a dual variable; z_i^{s-1} represents the expected position and heading of ASV i that the coordinator send at iteration $s-1$; $\cdot^s$ is the value of the corresponding variable at iteration s.

2: The coordinator:

(a) Calculates the expected trajectory of the object (z_i^{*s}) according to $\eta_i^s(k)$, the predicted trajectory of ASV i.

(b) Sloves the following problem and updates the predicted trajectory of the object:

$$\tau^{*s}(k) := \underset{\tau^*(k)}{\arg\min}\, J^*\left(\tau^*(k)\right) + \sum_{i=1}^{3}\left(-\lambda_i^{s-1}(k)'\tau^*(k) + \rho_i/2 \ \left\|z_i^{*s}(k) - \eta_i(k)\right\|_2^2\right);$$
$$\text{subject to (27)-(33).}$$

(c) Calculates the expected position and heading z_i^s of each ASV according to $z_i^{*s}(k)$ and updates the forces each ASV should provide.

3: ASV controller i updates the local dual variable with the information from the coordinator:

$$\lambda_i^s(k) := \lambda_i^{s-1}(k) + \rho_i\left(\eta_i^s(k) - z_i^s(k)\right),$$

and the primal and dual residual and tolerance:

$$\begin{aligned}
R_{\text{pri},i}^s(k) &:= \eta_i^s(k) - z_i^s(k),\\
R_{\text{dual},i}^s(k) &:= z_i^s(k) - z_i^{s-1}(k),\\
\varepsilon_{\text{pri},i}^s(k) &:= \sqrt{Nn_u}\varepsilon^{\text{abs}} + \varepsilon^{\text{rel}}\max\left\{\left\|\eta_i^s(k)\right\|_2, \left\|z_i^s(k)\right\|_2\right\},\\
\varepsilon_{\text{dual},i}^s(k) &:= \sqrt{Nn_u}\varepsilon^{\text{abs}} + \varepsilon^{\text{rel}}\left\|\lambda_i^s(k)\right\|_2.
\end{aligned}$$

4: ASV controllers and the coordinator move on to the next iteration s+1 and repeat Step 1 to Step 3 until following stopping condition is satisfied for all the ASV controllers and the coordinator:

$$\left\|R_{\text{pri},i}^s(k)\right\|_2 \leqslant \varepsilon_{pri,i}^s(k) \text{ and } \left\|R_{\text{dual},i}^s(k)\right\|_2 \leqslant \varepsilon_{\text{dual},i}^s(k).$$

4.1. Set up

The scenario we consider involves three ASVs that transport a floating object (e.g., a non-autonomous large vessel) from the North Sea to a terminal in the Port of Rotterdam, as shown in Figure 6. The ASVs have to transport the object following the path indicated by waypoints. An obstacle, e.g., a disabled vessel at anchor, is located on the reference path. In the port, so-called waterborne AGVs are employed for inter-terminal transport [32]. The waterborne AGV (Automated Guided Vehicles) is set as sailing with a constant speed, 0.35 m/s with higher priority than the proposed object transport system. The reference path of the object to be moved has overlap with the Waterborne AGV path, as indicated in Figure 6. When encountering with the waterborne AGV, the proposed cooperative ASVs should give way. The coordinates of the waypoints, obstacle, and waterborne AGV path are provided in Table 1.

Two cases are considered in the simulation:

- Constant configuration: in this case, the towlines are regarded as straight lines ignoring the mass. The related

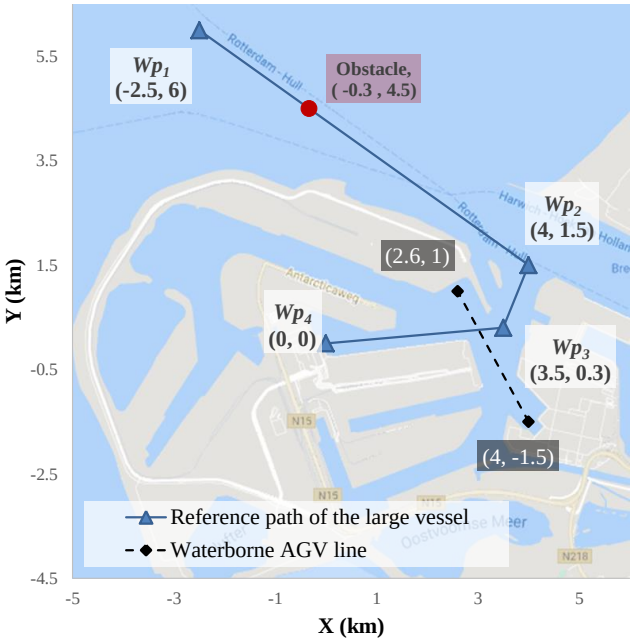

Figure 6: Reference paths in the simulations.

Table 1: Waypoints and the position of the obstacle

Coordinates	Waypoint	X (km)	Y (km)
Reference path	Wp_1	-2.5	6
	Wp_2	4	1.5
	Wp_3	3.5	0.3
	Wp_4	0	0
Static obstacle		-0.3	4.5
Waterborne AGV	Origin	2.6	1
	Destination	4	-1.5

distances between ASVs and the object are predetermined as 1.255/2 m for ASV 1, 2 and 1.255 m for ASV 3.

- Time-varying configuration: in this case, the related distances between the ASV 1, 2 and the object are determined by the towline model, (6) and (7), and the relative positions between the ASV 3 and the object is 1.255 m.

For the ASVs, the parameters of the model are scaled-up according to the Froude scaling law with a scaling factor $\chi = 1 : 100$. According to the scaling law, the multiplication factors for length, force, moment and time are χ, χ^3, χ^4, and $\sqrt{\chi}$, respectively. For the object, the scale factor is 1:200 when calculating related data. Related parameters in the simulation are given in Table 2. The simulation results underneath are shown with $\chi = 1 : 100$.

4.2. Results and discussion

In the two cases, the trajectories of the ASVs and the object are similar. The trajectories of the ASVs and the object in case 1 are shown in Figure 7. The snapshots show how the ASVs avoid collision with the static obstacles and the Waterborne AGV while maintaining the required formation. Safety is further confirmed by Figure 8. For both the object and the ASVs, their distances with the static obstacle and the Waterborne AGV are larger than the corresponding safety distances.

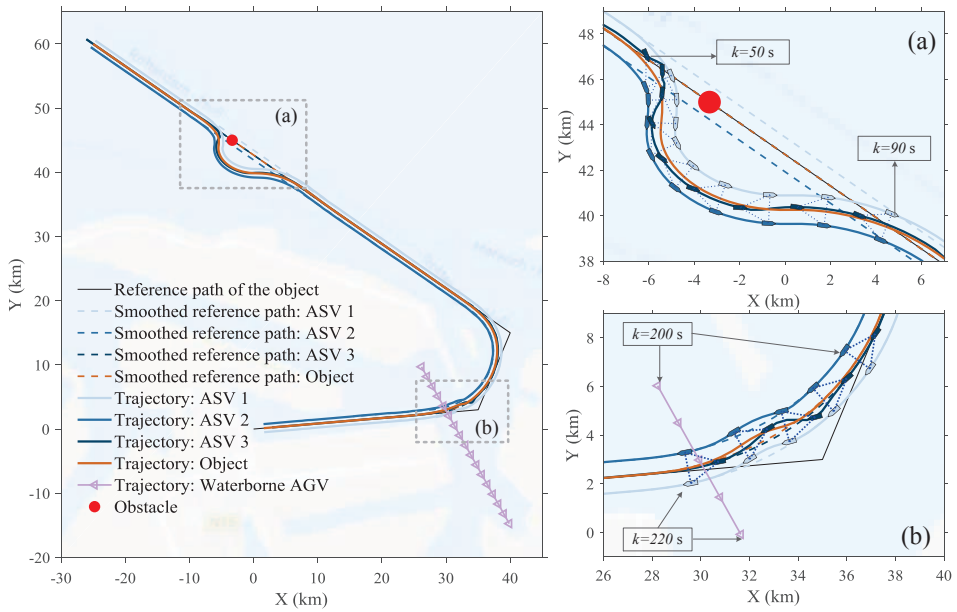

Figure 7: Trajectories of the ASVs and the object.

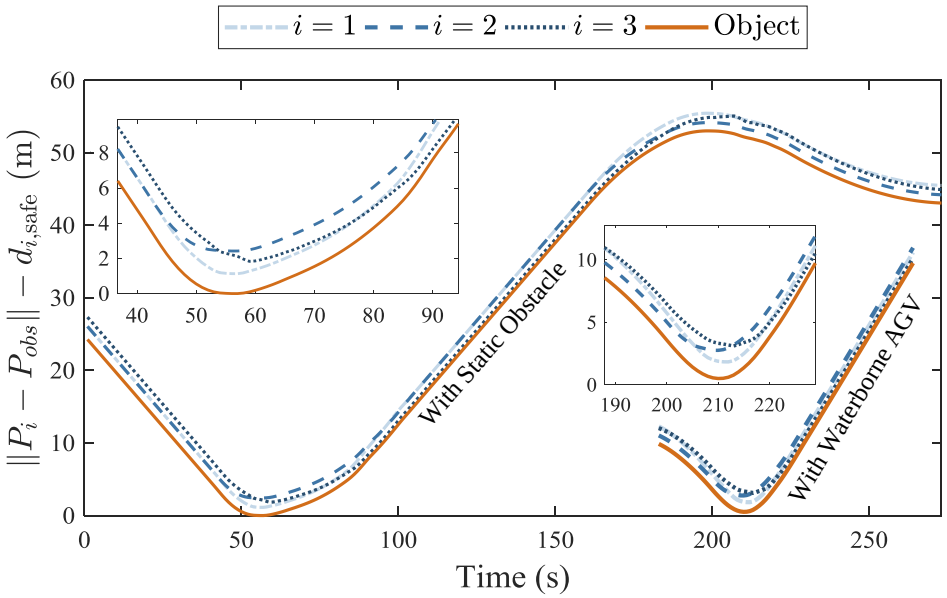

Figure 8: Distances with the static obstacle and the Waterborne AGV.

Table 2: Parameter setting

	Parameter	Value
ASV	Width	0.29 m
	Length	1.255 m
	$\nu_{\max}$	$[0.7, 0.7, 20\pi/180]^{\mathrm{T}}$
	$\nu_{\min}$	$[0, -0.7, -20\pi/180]^{\mathrm{T}}$
	$\tau_{\max} = -\tau_{\min}$	$[10, 10, 2]^{\mathrm{T}}$
	$d_{i,\mathrm{safe}}$	1.255/2 m
Object	Width	0.29×2 m
	Length	1.255×2 m
	$\nu_{\max}$	$[0.7, 0.7, 10\pi/180]^{\mathrm{T}}$
	$\nu_{\min}$	$[0, -0.7, -10\pi/180]^{\mathrm{T}}$
	$\tau_{\max} = -\tau_{\min}$	$[15, 15, 2]^{\mathrm{T}}$
	$d_{i,\mathrm{safe}}$	1.255×2 m
ASV configuration	$D_{1,2}^{\mathrm{ASV}}$	1.255/4 m
	L_3^{ASV}	1.255 m
	ω	25°
	$\theta_{\min}$	20°
	$\theta_{\min}$	30°
	$D_{\mathrm{H,min}}$	74 m
	$D_{\mathrm{H,max}}$	77 m
	$\varepsilon^{\mathrm{con}\dagger}$	$[0.01, 0.01, 0]^{\mathrm{T}}$
Towline (in full-scale)	L_R	76 m
	ϖ	12 kg/m
	EA	9.2×10^8 N
	$F_{\max}$	$2{\times}10^7$N
Trajectory generation	K	20 s
	$\hat{v}$	0.5 m/s
MPC controller design	H_{p}	10
	α	diag[10,10,50]
	γ	5
ADMM	$\varepsilon^{\mathrm{rel}}$	10^{-3}
	$\varepsilon^{\mathrm{abs}}$	10^{-3}

† The determination of the tolerances takes three factors into consideration: the linearization error analysis in Appendix A, the extension of a steel wire rope ($\leqslant 0.2\%$ the length [33]), and the computation time.

Figure 9 shows the path following performance of the proposed cooperative system. In both cases, mostly, the ASVs can move the object along the reference path. Deviations occur when the object and the ASVs have to depart from the path to avoid obstacles.

Figure 10 provides the distance between the ASVs and the object in the two cases. In the figure, $L_i^{\mathrm{ASV}}(k)$ is the required distance. When the towline model is considered, $L_i^{\mathrm{ASV}}(k)^2 = D_{\mathrm{H},i}^{\mathrm{fore}}(k)^2 + D_{\mathrm{tie}}^2 - 2D_{\mathrm{H},i}^{\mathrm{fore}}(k)D_{\mathrm{tie}} \cos\left(\theta_i^{\mathrm{fore}}(k) + \omega\right)$. In the case that the ASVs have a constant configuration (Figure 10(a)), the ASVs can keep the required distances with the object when the object is following a straight path. When turning actions are needed, such as for collision avoidance, deviations arise. However, the deviations are all within the predetermined tolerance. On the contrary, when the required configuration is changing according to the towline model, the differences between the actual distances and the required distances always exit, see Figure 10(b).

The differences between the heading of the ASVs and the object are shown in Figure 11. Mostly, the headings of

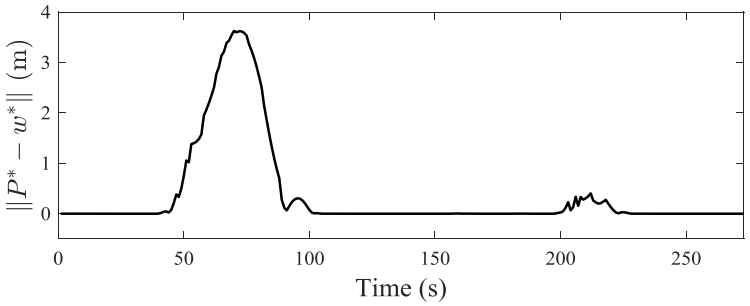

Figure 9: Tracking error of the object.

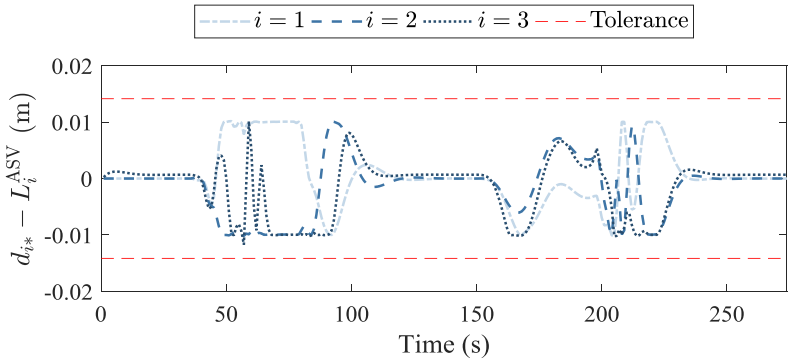

(a) Relative distance between ASVs and the object with a constant configuration.

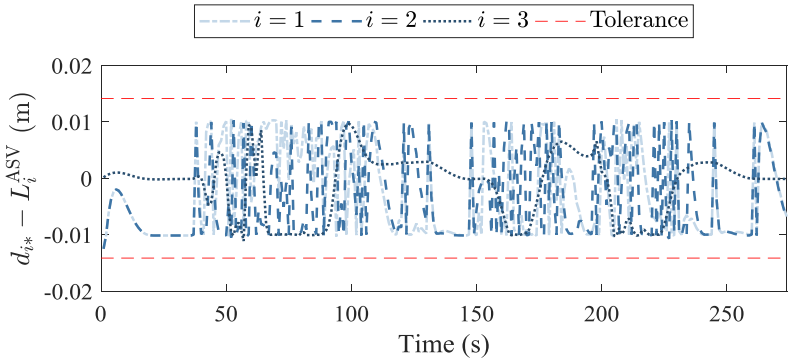

(b) Relative distance between ASVs and the object with a time-variying configuration.

Figure 10: Relative distance distance between ASVs and the object.

the three ASVs stay aligned with the heading of the object with small deviations. When the sharp turning is needed, e.g., at time step k = 56 s, ASV 3 have larger differences in heading with the object than the other two ASVs. This is mainly because the distance between ASV 3 and the object is larger than the others. The state changes of the object are enlarged when calculating the expected trajectory of ASV 3. Thus, ASV 3 needs larger changes in position and headings than ASV 1 and ASV 2 for configuration keeping.

Figure 12 provides the forces along the towlines. To produce the required forces, the horizontal distance between the two ends of each towline, ranging from 73 m to 77 m, and angles between the towlines and the object, ranging

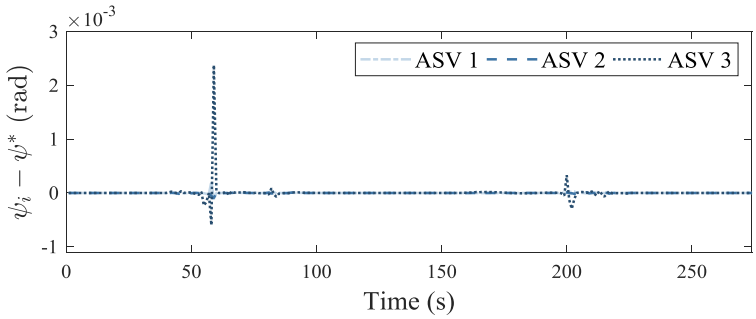

(a) Heading differences between each ASV and the object with a constant configuration.

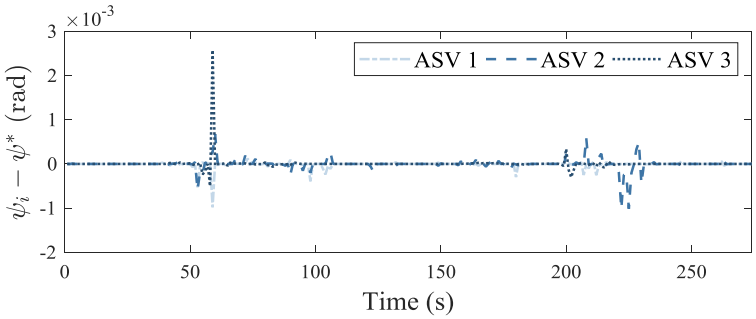

(b) Heading differences between each ASV and the object with a time-variying configuration.

Figure 11: Formation keeping performance.

from 20 ° to 30 °, change accordingly, see Figure 13 and 14.

Figure 15 shows the number of iterations and computation time needed for the ASVs to achieve consensus at each time step. If the reference related positions between the ASVs and the object are constant (Figure 15(a)), mostly, agreements are achieved in two iterations, within 1 s, which is shorter than the sampling time, 1 s in simulation and 10 s in full scale. The short computation time shows the potential to apply the proposed cooperative framework in reality. At time step k, the first solution each ASV finds is an extension of the solution at time step $k-1$. That is to say, an ASV prefers to follow the trajectories that it sends to other controllers. This property can also be used to deal with the communication delays, packet loss or connection failure: a controller i can assume that an ASV j follows the predicted trajectories it broadcast at time step k until the controller i receives an update on the state of ASV j. However, if the nonlinear towline model is integrated into the framework, the computation time increased dramatically, see Figure 15(b). The computation time does not have the same trend with the number of iterations any more. The most time-consuming part is to solve the nonlinear control allocation problem. Some methods may help to meet the real-time requirement under this circumstance, such as adopting a sampling time that is larger than the computation time or using a more suitable optimization algorithm or a computer with stronger calculation capability.

The time step $k = 124$ s is one of the steps in which most iterations are needed to obtain agreements when the ASVs have a time-varying configuration. Figure 16 shows how the primal and dual residuals evolve over iterations at this time step. The primal residual records the differences between the expected trajectory and the predicted trajectory, i.e., $\left\|\eta_i^s - z_i^s\right\|^2$. The dual residual records the differences between the expected trajectory at iteration s and the expected trajectory at iteration $s-1$, i.e., $\left\|z_i^s - z_i^{s-1}\right\|^2$. Through iterative negotiations, both primal and dual residuals decrease and finally meet the stopping criteria.

The linear and angular velocities of the object and ASVs are given in Figure 17. Surge and sway velocities of the ASVs and the object are the same when they are on the straight path. However, when the object takes turning actions, to keep the formation, the ASVs at different positions have to accelerate or decelerate accordingly.

Figure 18 and Figure 19 show the forces and moment each ASV provide. The solid red lines are the forces and

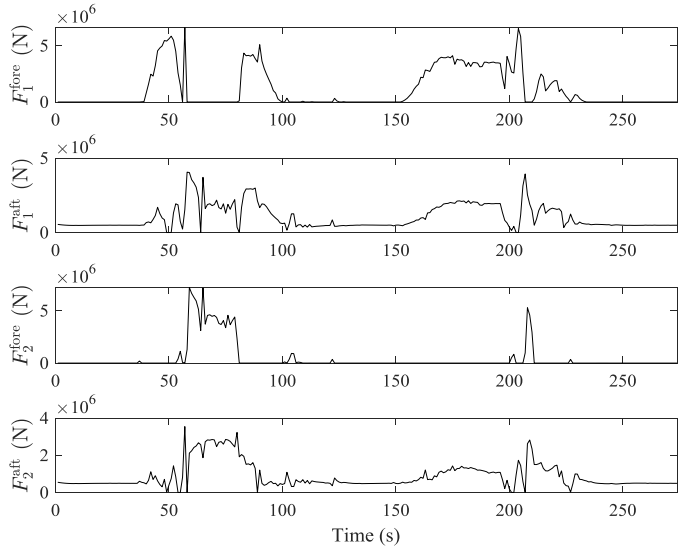

Figure 12: Forces along the towlines.

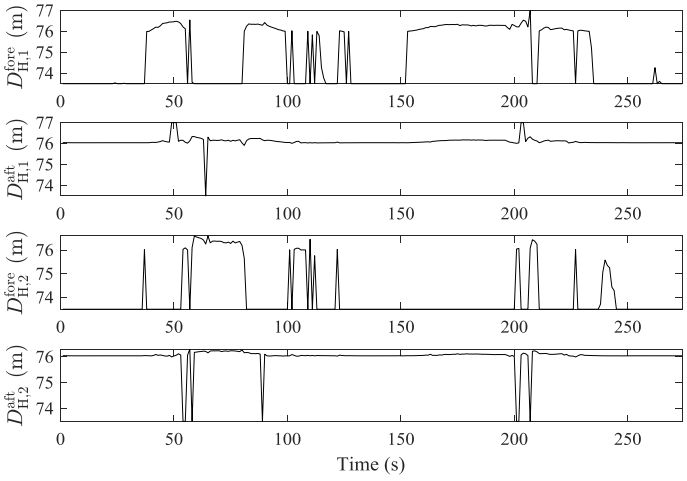

Figure 13: Horizontal distance between the two ends of each towline.

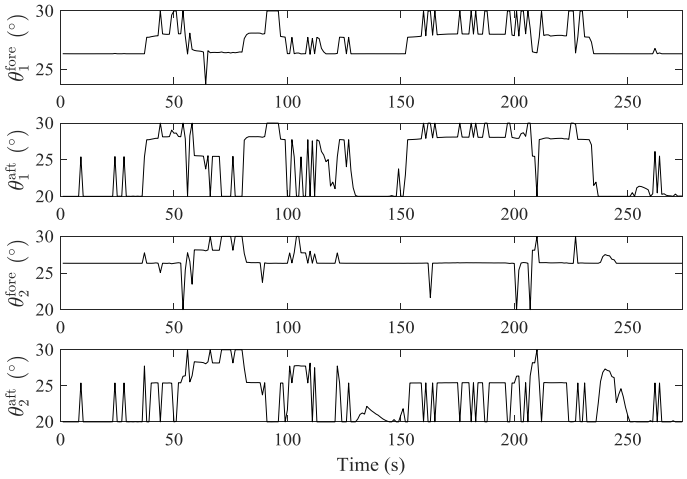

Figure 14: Angles between the towlines and the central line of the object.

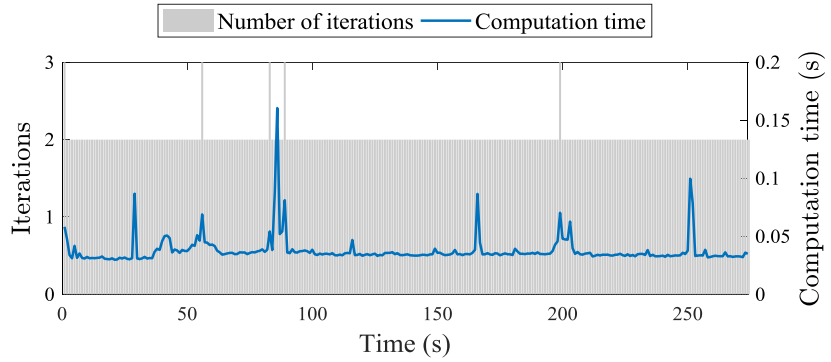

(a) Computation time and number of iterations with a constant configuration.

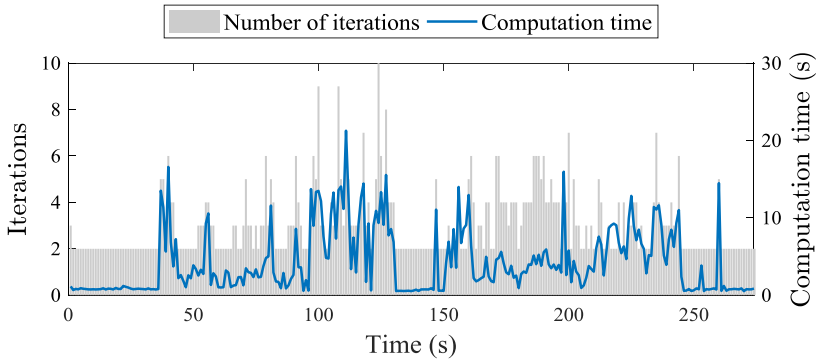

(b) Computation time and number of iterations with a time-varing configuration.

Figure 15: Computation time and number of iterations.

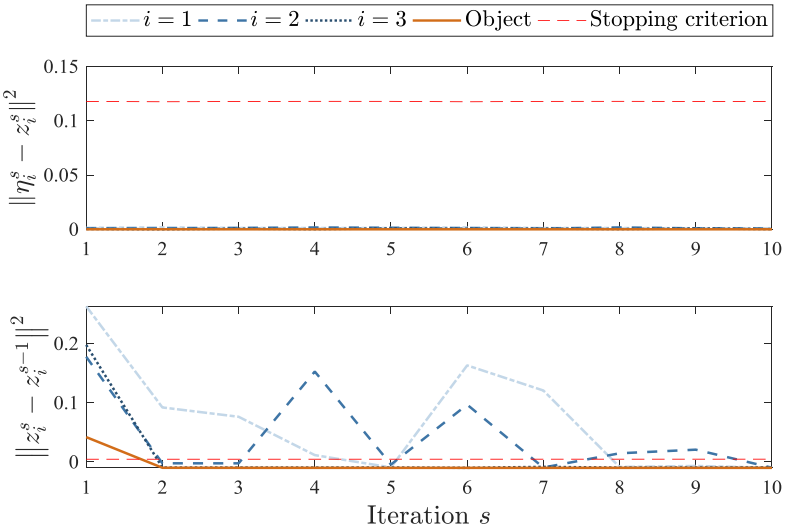

Figure 16: Evolution of the primal and dual residual at time step k = 124 s with a time-varing configuration.

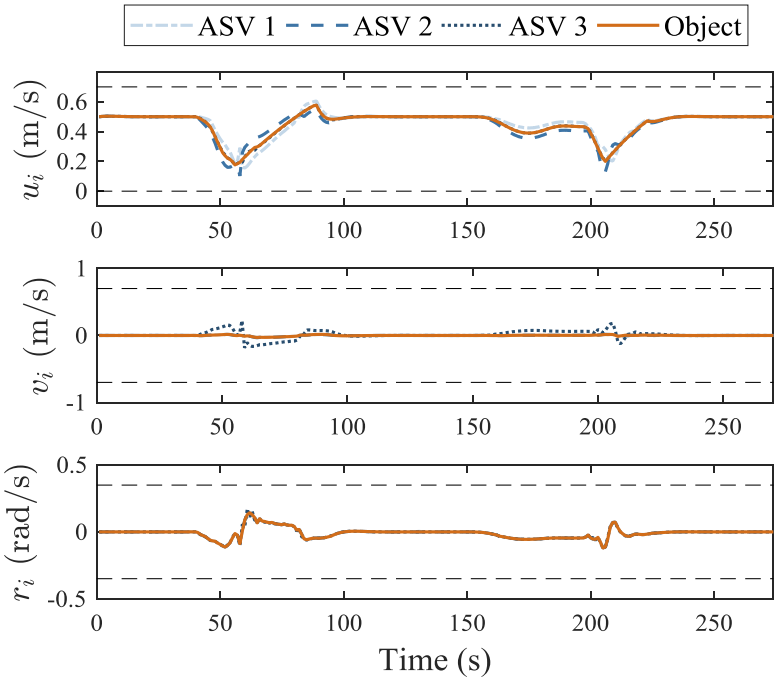

(a) Linear and angular velocities of the ASVs and the object with a constant configuration.

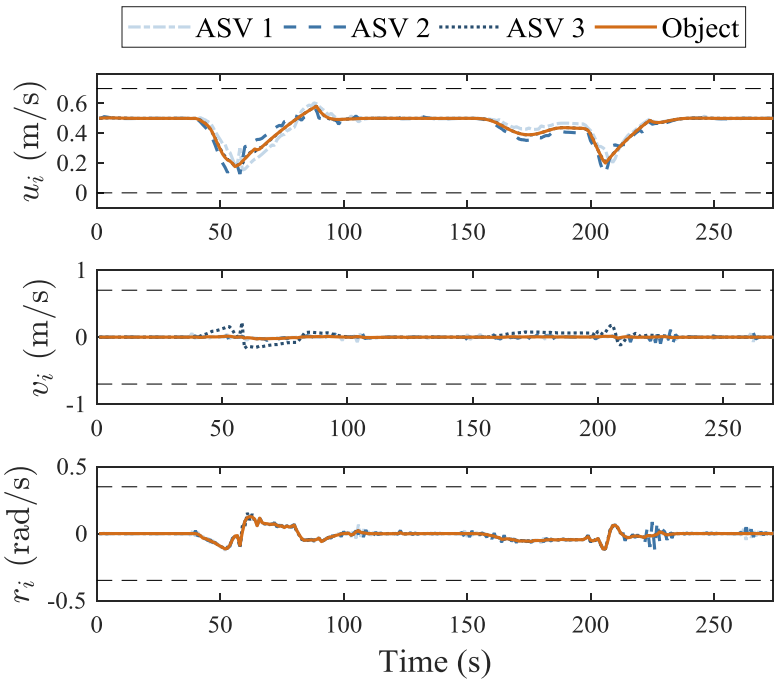

(b) Linear and angular velocities of the ASVs and the object with a time-varing configuration.

Figure 17: Linear and angular velocities of the ASVs and the object.

moment, including the forces to move the objects and the forces and moment an ASV need to keep formation (the blue dot lines). The limitations on maximum and minimum forces and moments are all met. The results indicate that ASV 3 is the main source which provides the surge force for the object, while ASV 1 and 2 provide the moment when turning actions are needed.

5. Conclusions and future research

This paper focuses on cooperative floating object transport, i.e., a group of ASVs coordinate their actions to transport floating objects. We propose a formation-based cooperative object transport system with a multi-layer control structure. The cooperative transport problem is divided into three sub-problems, trajectory tracking of the object, control allocation, and formation tracking of the ASVs. MPC controllers with a successively linearized prediction model are designed for distributed control of ASVs and the object. A negotiation framework based on ADMM is employed to achieve consensus among the ASVs. The errors introduced by the successively linearized model with numerical simulations. A simulation involving moving a large vessel sailing inbound the Port of Rotterdam is carried out to show the effectiveness of the proposed cooperative framework. The results show that the proposed cooperative system can transport the floating object along a predefined trajectory and avoid potential static and dynamic obstacles. Ultimately, this leads to methods that can also become useful for moving large vessels, barges, and off-shore platforms in future ports where both human-operated and autonomous vessels exist.

Further research will consider the following directions. Firstly, although the predictive property of MPC benefits the control of the ASVs under disturbances, more efforts are needed to analyze the influences of external disturbances. Methods that take the influences into consideration, such as Robust MPC and Stochastic MPC, could be developed in future research. Secondly, formal recursive feasibility and stability analysis for the proposed method can be investigated besides the numerical approach considered here. Thirdly, in this paper, as well as in much existing research for ASVs, the effectiveness of the methods are assessed through simulations. Physical simulations can be carried out to make steps towards real-world application.

Appendix A. Linearization errors

The successively linearized model introduced in Section 3.2.1 is based on Taylor's theorem. Therefore, the accuracy of the approximation is influenced by the differences between the seed state and reference state that the controllers want to follow. We carry out an analysis on the errors that are brought by linearization. The linearization error is defined hereby as the difference between the position P_l calculated with the linearized model (8), and the position P_{nl} calculated with the non-linear model (3).

In the simulations, we use the CyberShip 2 model to represent the dynamics of the ASV. The motion of the ASV is controlled by the proposed MPC controller. Related parameters are given in Table 2.

Two scenarios are considered to analyze the accuracy of the approximation of the successively linearized model.

- Scenario 1: Impacts of initial seed state

  The ASV follows the different paths with the same successively linearized model with the same seed state at the first time step. The reference paths are shown in Figure 20(a). The angle between the seed trajectory and the reference path increases from 0° to 180° with an interval of 10°.

- Scenario 2: Impacts of turning angles

  The reference path that the ASV needs to follow has a turning angle increasing from 0° to 180° at an interval of 10°, as shown in Figure 20(b).

Results of Scenario 1 are presented in Figure A.21. In this case, the maximum linearization error arises in the first time step. The maximum linearization errors in the situation that the ASV follows different reference paths are presented in Figure 21(a). The maximum error increases when the angle between the seed path and the reference path increases. However, the successive linearization method can make use of the most up-to-date information and adapt the linear model according to the control input determined in the first time step. In this way, the deviations between

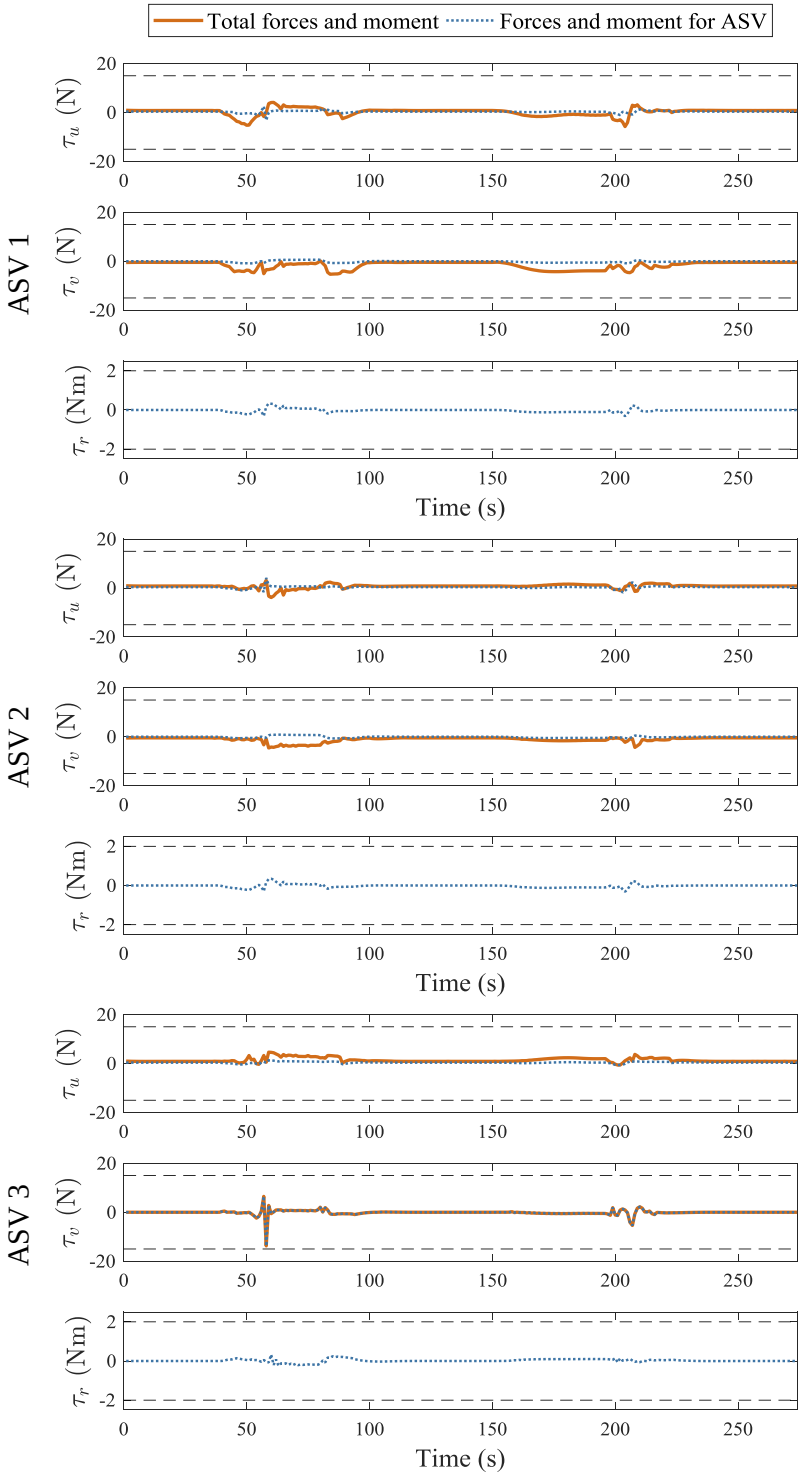

Figure 18: Forces and moment of each ASV with a constant configuration.

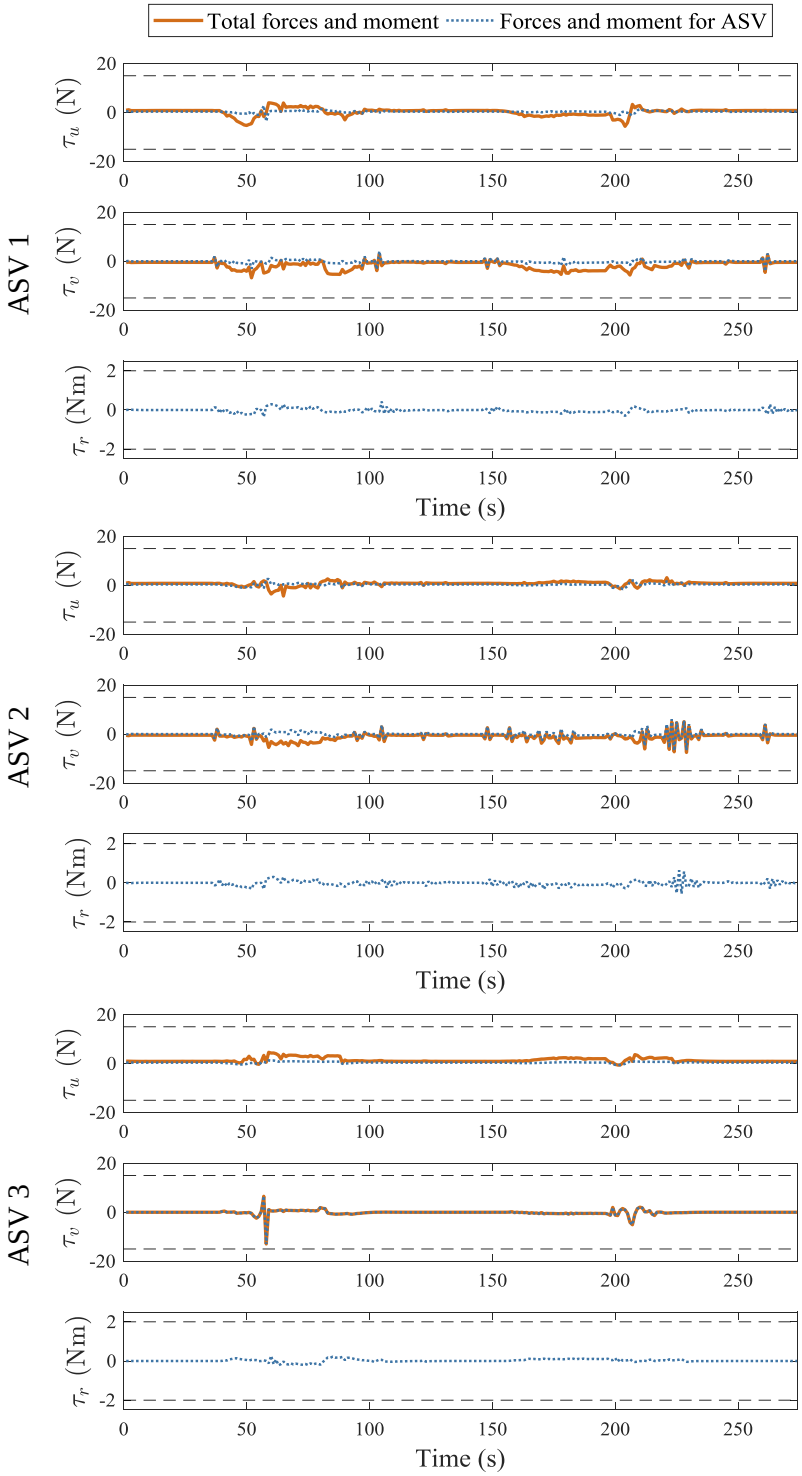

Figure 19: Forces and moment of each ASV with a time-varying configuration.

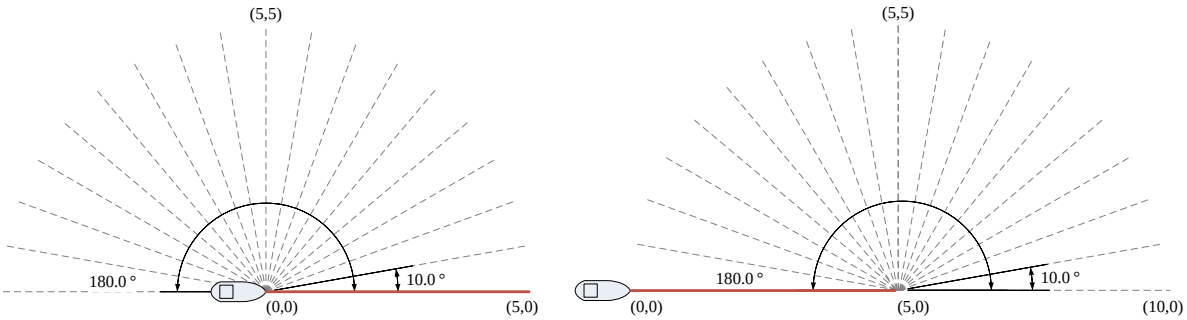

(a) Reference paths in Scenario 1

(b) Reference paths in Scenario 2

Figure A.20: Reference paths in the simulations (The thick red line is the seed trajectory for linearization in the first time step)

the seed path and reference path become smaller. Thus, the linearization error reduces dramatically in the second time step, see Figure 21(b).

Simulation results for Scenario 2 are presented in Figure A.22. Figure 22(a) shows an increasing tendency the maximum error with the turning angle. Large linearization errors arise when the ASV take turning actions, see Figure 22(b). The main reason is that the differences between the seed state and reference state become larger at the moment when the controllers decide to take turning actions. Nevertheless, the errors are small during the simulations.

To conclude, the accuracy of the successively linearized model is influenced by two factors: the differences between the seed state and the reference state, and the smoothness of the reference path. Owing to the property of making use of the latest state of the system, the successively linearized model can make adjustments quickly. This property provides the linearized model the required accuracy for the motion control of ASVs.

Acknowledgment

This research is supported by the China Scholarship Council under Grant 201406950041.

List of Symbols

In this paper, A variable followed by $(k+l|k)$, i.e., $\tau_i(k+l|k)$, indicates the prediction of the variable at time step $k+l$ made at time step k; $\cdot^s$ indicates the value of the corresponding variable at iteration s. Below follows a list of symbols and notations.

A	cross-sectional area of the towline
A_i^d, B_i^d	Jacobian matrices
C_i	Coriolis-centripetal matrix, including rigid-body and added mass Coriolis-centripetal matrices
$d_{i,j\|i}$	distance between ASV i and ASV j calculated by ASV i
$d_{*i\|*}$	distance between ASV i and the object with the information sent by ASV i
d_{safe}	safety distance of ASV i
$d_{*i,\text{safe}}$	safety distance of the object
$D_{\text{H},1}^{\text{fore}}$	horizontal distance between the two ends of the towline
D_i	damping force of ASV i
E	Young's modulus of the towline
$F = \left[F_1^{\text{fore}}, F_1^{\text{aft}}, F_2^{\text{fore}}, F_2^{\text{aft}}, F_3^{\text{stern}}\right]^{\text{T}}$	forces along the towlines on the horizontal plane
θ_i^{fore}, θ_i^{aft}	angles between the towlines and central line of the object
F_i^u, F_i^v	forces that ASV i should provide
$F_{\max}$	maximum forces on the towline

G_R	gravity of the towline
$h_i(\cdot)$	geometric relation between the object and the ASVs considering the desired formation and the towline model
H_p	prediction horizon
l	lth time step in the prediction horizon
L^tie	distance from the center of mass of the object to the segment between the ties
L_R	length of the towline
M_i	system inertia matrix, including rigid-body and added mass matrices
P_i, P^*	position of the ASVs and the object
$P_{i\|*}$	position of the ASV i that the object received
$R(\psi_i)$	a rotation matrix between body-fix frame of ASV i and the North-East-Down
R_pri, R_dual	primal and dual residual
T_1^fore	tension in the horizontal direction
$\breve{T}_1^\mathrm{fore}$	tension on the towline
$\mathrm{T}_i(\psi_i, \psi^*)$	transformation matrix between forces along the towline and the forces ASV i provided
$\hat{v}$	a constant speed to generate the reference path
w_i	reference state pf ASV i
Wp_i	a waypoint
	forces to control the motion of the object
x^e, τ^e	seed state and seed input for successively linearized model
x_i, τ_i	state and input of ASV i
x^*, τ^*	state and input of the object
z_i^*	expected trajectory of the ASV i that calculated according to the predicted trajectory of the object
z_i	expected trajectory of the object that calculated according to the predicted trajectory of ASV i
α, γ	weights in the objective function
χ	scaling factor
$\eta_i = [p_i, q_i, \psi_i]^\mathrm{T}$	coordinates p_i, q_i, and heading angle ψ_i in the North-East-Down coordinate system
$\nu_i = [u_i, v_i, r_i]^\mathrm{T}$	surge and sway velocities u_i, v_i, and yaw rate r_i in Body-fixed reference frame
Γ	transformation matrix between τ^* and F
λ_i	dual variable
ω	angle of the segment between two ties and the center of mass of the object
ρ_i	penalty parameter
ϖ	density of the towline
ε^abs, ε^rel	absolute tolerance and relative tolerance
ε_pri, $\varepsilon_\mathrm{dual}$	feasibility tolerances for primal and dual residuals
Ξ	a set of position in navigable waters

References

References

[1] Z. Liu, Y. Zhang, X. Yu, C. Yuan, Unmanned surface vehicles: An overview of developments and challenges, Annual Reviews in Control 41 (2016) 71 – 93.

[2] M. Schiaretti, L. Chen, R. R. Negenborn, Survey on autonomous surface vessels: Part II - categorization of 60 prototypes and future applications, in: T. Bektaş, S. Coniglio, A. Martinez-Sykora, S. Voß (Eds.), Computational Logistics, Springer, Springer International Publishing, 2017, pp. 234–252.

[3] L. Chen, H. Hopman, R. R. Negenborn, Distributed model predictive control for vessel train formations of cooperative multi-vessel systems, Transportation Research Part C: Emerging Technologies 92 (2018) 101–118.

[4] Y. Lu, G. Zhang, Z. Sun, W. Zhang, Robust adaptive formation control of underactuated autonomous surface vessels based on mlp and dob, Nonlinear Dynamics 94 (1) (2018) 503–519.

[5] Y. Huang, L. Chen, P. van Gelder, Generalized velocity obstacle algorithm for preventing ship collisions at sea, Ocean Engineering 173 (2019) 142 – 156.

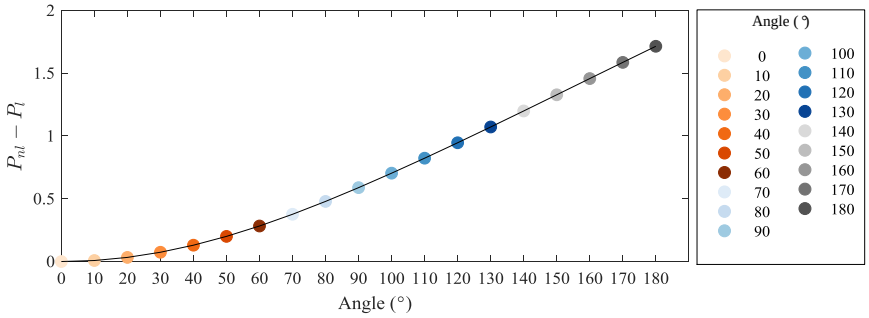

(a) Maximum linearization error (the first time step) in Scenario 1

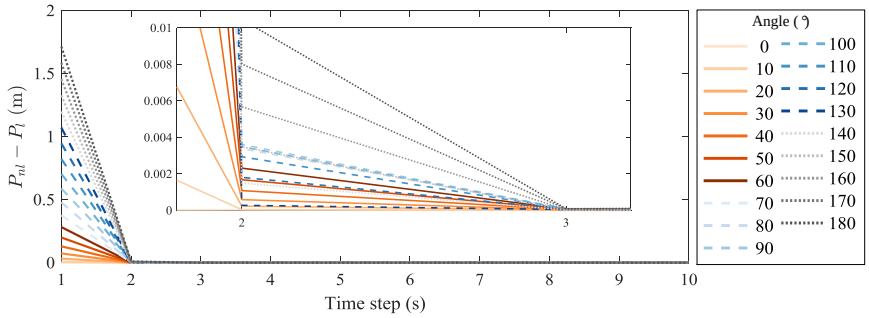

(b) Linearization error in each time step in Scenario 1

Figure A.21: Simulation results for Scenario 1

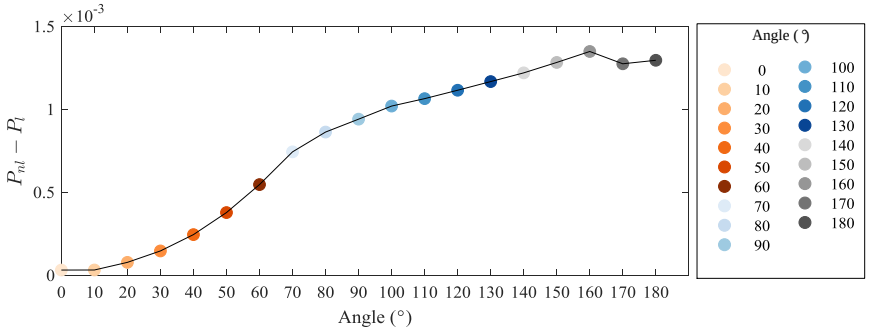

(a) Maximum linearization error in Scenario 2

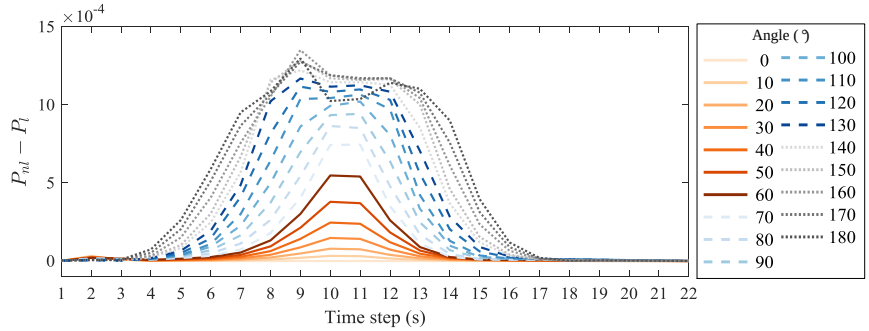

(b) Linearization error in each time step in Scenario 2

Figure A.22: Simulation results for Scenario 2

[6] S. Li, J. Liu, R. R. Negenborn, Distributed coordination for collision avoidance of multiple ships considering ship maneuverability, Ocean Engineering 181 (2019) 212 – 226.
[7] E. Tuci, M. H. M. Alkilabi, O. Akanyeti, Cooperative object transport in multi-robot systems: A review of the state-of-the-art, Frontiers in Robotics and AI 5 (2018) 59.
[8] J. Ota, Multi-agent robot systems as distributed autonomous systems, Advanced Engineering Informatics 20 (1) (2006) 59 – 70.
[9] T. I. Fossen, Handbook of marine craft hydrodynamics and motion control, John Wiley & Sons Ltd, United Kingdom, 2011.
[10] D. Braganza, M. Feemster, D. Dawson, Positioning of large surface vessels using multiple tugboats, in: Proceedings of the 2007 American Control Conference, 2007, pp. 912–917.
[11] J. Esposito, M. Feemster, E. Smith, Cooperative manipulation on the water using a swarm of autonomous tugboats, in: Proceedings of 2008 IEEE International Conference on Robotics and Automation, Pasadena, California, 2008, pp. 1501–1506.
[12] B. Bidikli, E. Tatlicioglu, E. Zergeroglu, Robust dynamic positioning of surface vessels via multiple unidirectional tugboats, Ocean Engineering 113 (2016) 237 – 245.
[13] M. Feemster, J. Esposito, J. Nicholson, Manipulation of large objects by swarms of autonomous marine vehicles. Part 1-rotation, in: Proceedings of the 38th Southeastern Symposium on System Theory, TN, USA, March 5-7, 2006, pp. 255–259.
[14] K.-K. Oh, M.-C. Park, H.-S. Ahn, A survey of multi-agent formation control, Automatica 53 (2015) 424 – 440.
[15] Y. Liu, R. Bucknall, A survey of formation control and motion planning of multiple unmanned vehicles, Robotica 36 (7) (2018) 1019–1047.
[16] C. F. L. Thorvaldsen, R. Skjetne, Formation control of fully-actuated marine vessels using group agreement protocols, in: 2011 50th IEEE Conference on Decision and Control and European Control Conference, 2011, pp. 4132–4139.
[17] L. Liu, D. Wang, Z. Peng, T. Li, Modular adaptive control for los-based cooperative path maneuvering of multiple underactuated autonomous surface vehicles, IEEE Transactions on Systems, Man, and Cybernetics: Systems 47 (7) (2017) 1613–1624.
[18] Y. Lu, G. Zhang, Z. Sun, W. Zhang, Adaptive cooperative formation control of autonomous surface vessels with uncertain dynamics and external disturbances, Ocean Engineering 167 (2018) 36 – 44.
[19] A. Fitriadhy, H. Yasukawa, Course stability of a ship towing system, Ship Technology Research 58 (1) (2011) 4–23.
[20] J. Tao, L. Du, M. Dehmer, Y. Wen, G. Xie, Q. Zhou, Path following control for towing system of cylindrical drilling platform in presence of disturbances and uncertainties, ISA Transactions.
[21] D. Q. Mayne, Model predictive control: Recent developments and future promise, Automatica 50 (12) (2014) 2967 – 2986.
[22] R. R. Negenborn, J. M. Maestre, Distributed Model Predictive Control: An overview and roadmap of future research opportunities, Control Systems 34 (4) (2014) 87–97.
[23] J. B. Rawlings, D. Q. Mayne, Model Predictive Control: Theory and Design, Madison, USA: Nob Hill Publishing, 2015.
[24] H. Zheng, R. R. Negenborn, G. Lodewijks, et al., Trajectory tracking of autonomous vessels using model predictive control, in: Proceedings of the 19th IFAC World Congress, 2014.
[25] H. Zheng, R. R. Negenborn, G. Lodewijks, Predictive path following with arrival time awareness for waterborne AGVs, Transportation Research Part C: Emerging Technologies 70 (2016) 214–237.
[26] Y. Huang, L. Chen, P. Chen, P. H. . A. J. M. van Gelder, Ship collision avoidance methods: State-of-the-art, Safety Science.
[27] O. Schlichting, Ship resistance in water of limited depth - resistance of seagoing vessels in shallow water, Jahrbuch der STG 35 (1934) 127–148.
[28] J. Liu, R. Hekkenberg, E. Rotteveel, J. J. Hopman, Literature review on evaluation and prediction methods of inland vessel manoeuvrability, Ocean Engineering 106 (2015) 458 – 471.
[29] J. A. Long, Kinematic interpolation of movement data, International Journal of Geographical Information Science 30 (5) (2016) 854–868.
[30] S. Boyd, N. Parikh, E. Chu, B. Peleato, J. Eckstein, Distributed optimization and statistical learning via the alternating direction method of multipliers, Foundations and Trends in Machine Learning 3 (1) (2011) 1–122.
[31] A. Wächter, L. T. Biegler, On the implementation of an interior-point filter line-search algorithm for large-scale nonlinear programming, Mathematical Programming 106 (1) (2006) 25–57.
[32] H. Zheng, Coordination of waterborne AGVs, Ph.D. thesis, Delft University of Technology (2016).
[33] K. Feyrer, Wire ropes: Tension, Endurance, Reliability, Springer-Verlag Berlin Heidelberg, 2015.